ARTICLE

Intermolecular Vibrational Energy Transfers in Melts and Solutions

Yu-neng Shen[a,c], Bo Jiang[b], Chuan-qi Ge[a,d], Gang-hua Deng[a], Hai-long Chen[b], Xue-ming Yang[a], Kai-jun Yuan[a*], Jun-rong Zheng[b*]

a. State Key Laboratory of Molecular Reaction Dynamics, Dalian Institute of Chemical Physics, Chinese Academy of Sciences, Dalian 116023, China
b. Department of Chemistry, Rice University, Houston, Texas, USA
c. University of the Chinese Academy of Sciences, Beijing 100049, China
d. School of Physics and Electronic Technology, Liaoning Normal University, Dalian 116029, China

(Dated: Received on February 25, 2016; Accepted on April 6, 2016)

Resonant and nonresonant intermolecular vibrational energy transfers in GdmSCN/KSCN=1/1, GdmSCN/KS^{13}CN=1/1 and GdmSCN/KS^{13}C^{15}N=1/1 mixed crystals in melts and in aqueous solutions are studied with the two dimensional infrared spectroscopy. The energy transfers in the samples are slower with a larger energy donor/acceptor gap, independent of the Raman spectra. The energy gap dependences of the nonresonant energy transfers cannot be described by the phonon compensation mechanism. Instead, the experimental energy gap dependences can be quantitatively described by the dephasing mechanism. Temperature dependences of resonant and nonresonant energy transfer rates in the melts are also consistent with the prediction of the dephasing mechanism. The series of results suggest that the dephasing mechanism can be dominant not only in solutions, but also in melts (pure liquids without solvents), only if the molecular motions (translations and rotations) are much faster than the nonresonant energy transfer processes.

Key words: Vibrational energy transfers, 2D IR, Phonon compensation mechanism, Dephasing mechanism

I. INTRODUCTION

Vibrational energy transfer is of interest for a variety of reasons, most notably because of the importance of energy transfer processes in chemical transformations [1]. In particular, in condensed phases, whenever a molecular bond is broken, formed, or changed into another state, a large part of the energy involved in the processes inevitably comes from or converts into vibrational energy, the dynamics of which have been extensively studied in both theory and experiments for decades [2−27]. In addition, intermolecular vibrational energy transfer is also a key component of many important phenomena, *e.g.*, heat transportations and cell signaling. However, the quantitative description of intermolecular vibrational energy transfers in condensed phases remains a grand challenge, as intermolecular energy transfers are typically accompanied by intramolecular energy relaxations and many mechanisms can play roles simultaneously [6, 13, 28, 29].

In the past few years, a series of intermolecular vibrational energy transfer experiments in solutions and crystals were conducted [30−40]. From these experimental and theoretical studies, it was found that the dominant mechanism for both resonant and nonresonant intermolecular vibrational energy transfers [40, 41] (the definition of them can be found in the previous studies) in the solutions is not the long-believed phonon compensation mechanism [6]. Instead, it is the dephasing mechanism [40] that dictates the energy transfer processes. The essential difference between these two mechanisms is that in the phonon compensation mechanism the energy difference between the donor and acceptor is compensated by phonons (instantaneous low frequency normal modes) in the liquids. Therefore the energy transfer is not necessarily slower with a larger energy gap, but dependent on the relative phonon densities at each energy gap. While in the dephasing mechanism, energy can be transferred by molecules only when they are resonant (the donor and acceptor have the same frequency) [40]. In a condensed phase, because of molecular collisions, the energy (or frequency) of a molecule is constantly fluctuating. For two molecules of which the initial energies are different, they can exchange energy once their energies fluctuate to be the same. Because of the "resonant" nature, in the dephasing mechanism the energy transfer is slower with a larger initial energy gap since it is more difficult to overcome a larger gap by random molecular collisions. Here, a point needs to be emphasized. In the phonon compensation mechanism, during the energy transfer process, the donor

*Authors to whom correspondence should be addressed. E-mail: kjyuan@dicp.ac.cn, junrong@rice.edu

(D) and acceptor (A) energy values are different. The energy sum of donor plus phonon (P) is the same as that of the acceptor, assuming the energy of the donor is smaller. The process can be schematically described as D+P⇔A. In the dephasing mechanism, even if the initial energy values of the donor and acceptors are different, during the energy transfer process they are on resonance, because prior to transfer due to molecular collisions (C) they have fluctuated to be the same. This process can be described as $D+C_D \rightarrow D^* \Leftrightarrow A^* \leftarrow A+C_A$. Recently, we have derived an equation which can quantitatively describe the energy transfer rate constant for the dephasing mechanism [37−39],

$$k_{DA} = \frac{2}{1+\exp\left(-\frac{\Delta\omega_{DA}}{k_B T}\right)} V_{DA}^2 \frac{\tau^{-1}}{(\Delta\omega_{DA})^2 + 4V_{DA}^2 + \tau^{-2}} \quad (1)$$

where $\Delta\omega_{DA}=\omega_D-\omega_A$, the difference between the central energy (frequency) values of D and A, also termed as the donor/acceptor (D/A) energy gap (this value is equal to 0 for the resonant energy transfer). τ is the dephasing time of the coherence between the donor and acceptor. In converting the τ with the line width τ^{-1}, a factor of 2τ is needed, *e.g.* $\tau^{-1}=\frac{1}{2\pi}\frac{100}{3\tau}$ cm^{-1}. k_B is Boltzmann's constant, and T is the absolute temperature, k_BT is converted to wavenumber by being $0.69T$. V_{DA} is the D/A coupling strength which is quantitatively correlated to the donor/acceptor distance (r_{DA}) under the dipole/dipole interaction mechanism by [42]:

$$V_{DA}^2 = \frac{1}{n^4}\frac{\mu_D^2\mu_A^2}{(4\pi\varepsilon_0)^2}\frac{\kappa^2}{r_{DA}^6} \quad (2)$$

where n is the refractive index. μ_D and μ_A are the respective transition dipole moments of the donor and acceptor. ε_0 is the vacuum permittivity. r_{DA} is the distance between the donor and acceptor. κ is the orientation factor dependent on the relative orientations of the donor/acceptor and the relative time scales of the rotations of the donor/acceptor and the energy transfer. All parameters in Eq.(1) and Eq.(2) are experimentally accessible.

Our previous solution experiments in different solvents can be described by Eq.(1) and Eq.(2) very well [30−40]. However, experiments in a pure liquid (without solvents) on this topic has never been conducted. Is there any difference of energy transfer mechanism in liquid (*e.g.* molten salt) without solvents? According to our previous study [40], in a solution the efficiency of phonon compensation is diminished because the random molecular translation time scale is faster than the nonresonant energy transfer. The viscosity of a molten salt is much larger than that of a solution, and the transient local structure of a melt can be similar to that of the crystal. Under such scenario, it is conceivable that in a molten salt the efficiency of phonon compensation could be high and the phonon compensation mechanism could be important for nonresonant energy transfers, different from those in solutions. In this work, we conduct comparison studies on intermolecular vibrational energy transfers in a molten salt and its solutions to investigate this fundamental problem.

II. EXPERIMENTS

The experimental setup has been described elsewhere [30, 31, 43−45]. Briefly, the experimental setup consisted of a Ti:Sapphire oscillator (∼400 mW, ∼800 nm with a band width ∼45 nm, <35 fs, ∼76 MHz, LIGHTHOUSE PHOTONICS sprout combining QUANTRONIX Ti-Light), two Ti:Sapphire regenerative amplifiers and two optical parametric amplifier (OPA) systems. The oscillator pumps the two Ti:Sapphire regenerative amplifiers, 90% power entering a picosecond amplifier (∼3.5 W, ∼800 nm with a band width ∼0.6 nm, ∼1.3 ps, 1 kHz, QUANTRONIX Integra-C) and 10% to a femtosecond amplifier (∼3.5 W, ∼800 nm with a band width ∼26 nm, ∼40 fs, 1 kHz, QUANTRONIX Integra-C) respectively. We use ∼2.8 W of the picosecond amplifier to pump a picosecond OPA (TOPAS-800) plus non-collinear difference frequency generator (NDFG) system to producing ∼1.4 ps (vary from 1.0−1.5 ps in different frequencies) mid-IR pulses with a bandwidth ∼15 cm^{-1} in a tunable frequency range from 500 cm^{-1} to 4000 cm^{-1} with energy of 1−40 μJ/pulse at 1 kHz. We also use ∼2.8 W of the femtosecond amplifier to pump another femtosecond OPA(TOPAS-Prime) and NDFG system producing ∼140 fs mid-IR pulses with a bandwidth ∼200 cm^{-1} in a tunable frequency range from 500 cm^{-1} to 4000 cm^{-1} with energy of 1−40 μJ/pulse at 1 kHz. In the 2D IR experiments, the ps IR pulse excites the vibrations of the molecules and its excitation power is adjusted based on need. The fs IR pulse is the probe beam. It is frequency resolved by a spectrograph and then is collected on a 2×32 pixel mercury cadmium telluride detector (Infrared Associates) yielding the ω_m axis of a 2D spectrum. The optical resolution used was 4−7 cm^{-1} (depending on the used grating). Scanning the pump frequency yields the ω_τ axis of the spectrum. Two polarizers are inserted into the probe beam pathway, one is located immediately behind the sample to selectively measure the parallel or perpendicular polarized signal relative to the pump beam and the other is before the sample rotating the polarization of the probe pulse 45° with respect to that of the pump pulse. The entire system is computer controlled. The IR pump probe signal $P(t)$ is collected by measuring the transmission of the probe beam through the sample by chopping the pump beam at 500 Hz. For a given delay time t (the de-

DOI:10.1063/1674-0068/29/cjcp1602028

lay between the IR pump and the IR probe pulse was changed by changing the optical pathlength travelled using a translation stage), the IR pump probe signal is defined by:

$$P(t) = \frac{(I_{\text{pump-on}} - I_{\text{pump-off}})(t)}{I_{\text{pump-off}}} = \frac{\Delta I(t)}{I} \quad (3)$$

where I is the transmission of the probe beam. Vibrational lifetimes are obtained from the rotation-free signal,

$$P_{\text{life}} = P_{//} + 2P_{\perp} \quad (4)$$

where $P_{//}$ and $P_{\perp}$ are parallel and perpendicular data, respectively. Rotational relaxation time is acquired from $R=(P_{//}-P_{\perp})(P_{//}+2P_{\perp})$. The Raman spectra were taken from a commercial Raman spectrometer (BRUKER, SENTERRA RAMAN).

Guanidiniumthiocynate (GdmSCN) was purchased from Aladdin. KSCN, $KS^{13}CN$ and $KS^{13}C^{15}N$ were purchased from Aldrich and used as received. D_2O was purchased from C/D/N Isotopes Inc. GdmSCN/$KS^{13}CN$=1/1, GdmSCN/$KS^{13}C^{15}N$=1/1, GdmSCN/KSCN/$KS^{13}C^{15}N$=0.5/0.48/0.02, and GdmSCN/KSCN=1/1 mixed crystals were prepared by dissolving the components in methanol, and these were stirred for 0.5 h. The solvents were then removed under vacuum. The procedure was repeated three times, and then the components were uniformly mixed. GdmSCN/$KS^{13}CN$=1/1 and GdmSCN/$KS^{13}C^{15}N$=1/1 salts in D_2O saturated solutions were prepared by direct dissolution of the salts in water.

GdmSCN/$KS^{13}CN$=1/1, GdmSCN/$KS^{13}C^{15}N$=1/1, and GdmSCN/KSCN=1/1 aqueous saturated solutions and the mixed crystals in melts, used for the experimental measurements, were contained in a sample cell composed of two CaF_2 windows separated by a Teflon spacer. The thickness of the spacer was adjusted accordingly to the optical densities. Experiments of solutions were performed at 296 K, and that of melts at 403 and 473 K. All the experiments conducted at high temperature were achieved by a temperature controller connected with separate heater and sample thermocouples, and the highest temperature it can reach is below 480 K. It should be noted that the melting point of KSCN is 446 K, thus we cannot use it to do temperature dependent experiments. The melting point of GdmSCN is about 393 K , and we cannot buy the isotope labeled GdmSCN species, *e.g.* $GdmS^{13}C^{15}N$, and that's why we chose to use the GdmSCN/KSCN=1/1 system of which the melting point is below 403 K. Certainly, the intermolecular vibrational energy transfer mechanism will not be affected by the system we chose. In our experiment, 2% of $KS^{13}C^{15}N$ is added to the GdmSCN/KSCN=1/1 mixed crystal in melts and GdmSCN/KSCN=1/1 D_2O saturated solution for resonant energy rate measurements (shown below). The $^{13}C^{15}N$ shifts the vibrational frequency 76 cm^{-1} lower, and the orientational dynamics of these molecules can be conveniently monitored using the pump-probe spectroscopy.

III. RESULTS AND DISCUSSIONS

A. FTIR spectra of samples

Energy transfer systems of GdmSCN/$KS^{13}CN$=1/1 and GdmSCN/$KS^{13}C^{15}N$=1/1 salts in D_2O saturated solutions at 296 K and the salts in melts without solvents at 403 and 473 K were studied, respectively. In the samples, the vibrational energy of the nitrile stretch can resonantly and nonresonantly transfer among the three anions: SCN^-, $S^{13}CN^-$, and $S^{13}C^{15}N^-$. In the vibrational energy transfer experiments, the energy donor and acceptor are the nitrile stretches CN, ^{13}CN, and $^{13}C^{15}N$ of the anions [37, 40]. As displayed in Fig.1 (a)−(f), the vibrational frequency of the nitrile stretch 0-1 transition of SCN-in the D_2O saturated solution is about 2063 cm^{-1} at 296 K, in melts is about 2058 cm^{-1} at both temperatures. Those of $S^{13}CN^-$ and $S^{13}C^{15}N^-$ red shift for about 47 and 76 cm^{-1} respectively in each temperature in each type of samples because of their heavier masses.

As demonstrated previously [37, 40], the electronic properties including the nitrile stretch 0-1 transition dipole moments of the three anions are hardly affected by the isotope substitutions. Therefore measuring the vibrational energy transfers among them can explicitly reveal the donor/acceptor energy gap dependent energy transfer rates in the melt-state and D_2O saturated solutions at different temperatures.

B. Resonant and nonresonant energy transfers in melts at 403 K

To measure the nitrile stretch resonant vibrational energy transfer of which the energy gap $\Delta\omega$=0, we used the resonant energy transfer induced anisotropy decay method [33, 37, 38, 40, 41, 44, 45]. Figure 2 shows the anisotropy decay of the nitrile stretch $^{13}C^{15}N$ 1st excited state in the sample GdmSCN/KSCN/$KS^{13}C^{15}N$=0.5/0.48/0.02 and CN 1st excited state in the sample GdmSCN/KSCN=1/1 in melts at 403 K, respectively. In general, in our experiments [37, 40, 44], there are two major contributions to the signal anisotropy decay. One is the molecular rotation, and the other is the resonant energy transfer from one anion to another anion with the same frequency and random orientation. The nonresonant energy transfers between SCN^- and $S^{13}C^{15}N^-$ are too slow (compared to the anisotropy dynamics) to make any significant contributions to the anisotropy decay [33, 37, 38, 40, 44]. In the sample GdmSCN/KSCN/$KS^{13}C^{15}N$=0.5/0.48/0.02 in melt, the anisotropy decay of the $S^{13}C^{15}N^-$ signal is mostly caused by the molecular rotation be-

DOI:10.1063/1674-0068/29/cjcp1602028

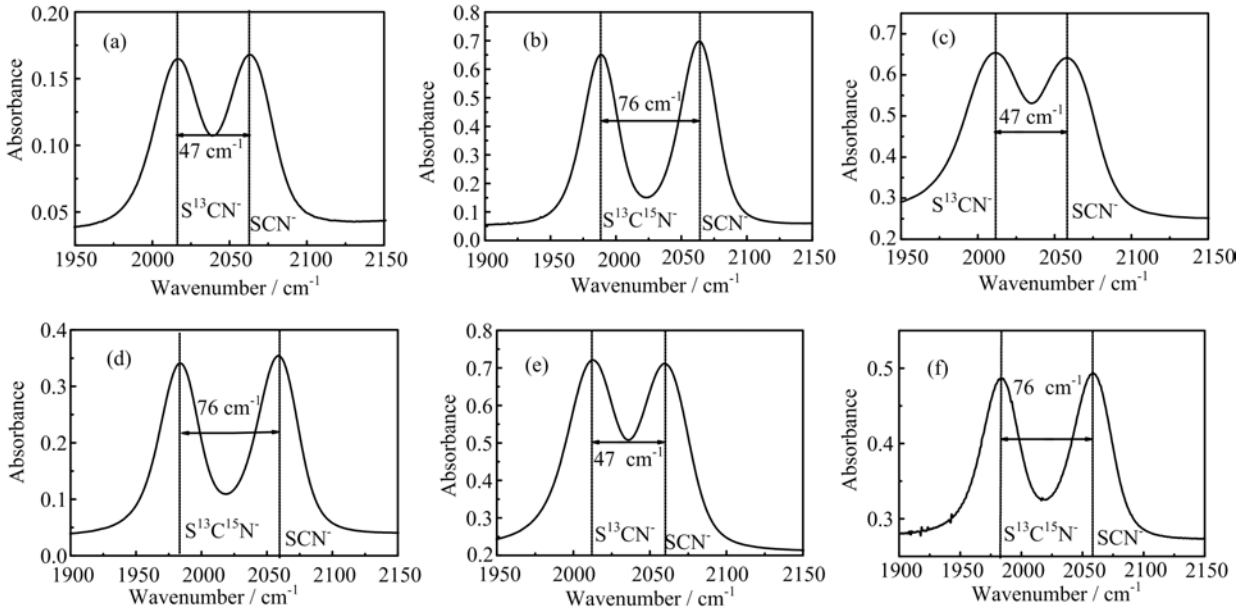

FIG. 1 (a) FTIR spectrum of the CN and ^{13}CN stretches of SCN^- and $S^{13}CN^-$ in a GdmSCN/KS^{13}CN=1/1 D_2O saturated solution at room temperature (296 K). The energy donor/acceptor gap is 47 cm^{-1}. (b) FTIR spectrum of the CN and $^{13}C^{15}N$ stretches of SCN^- and $S^{13}C^{15}N^-$ in a GdmSCN/KS^{13}C^{15}N=1/1 D_2O saturated solution at room temperature. The energy donor/acceptor gap is 76 cm^{-1}. FTIR spectra of (c) GdmSCN/KS^{13}CN=1/1 and (d) GdmSCN/KS^{13}C^{15}N=1/1 showing the nitrile stretch in melts at 403 K. FTIR spectra of (e) GdmSCN/KS^{13}CN=1/1 and (f) GdmSCN/KS^{13}C^{15}N=1/1 showing the nitrile stretch in melts at 473 K.

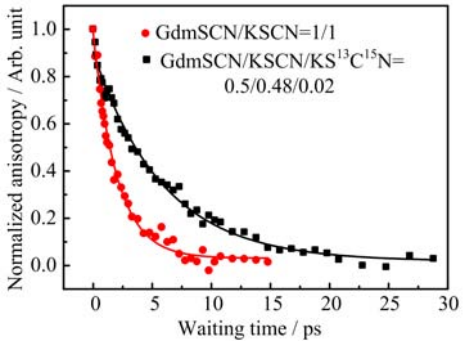

FIG. 2 Anisotropy decay data of $^{13}C^{15}N$ stretch 1st excited state of 2% KS^{13}C^{15}N in GdmSCN/KSCN/KS^{13}C^{15}N=0.5/0.48/0.02 mixed crystal in melts at 403 K, and that of CN stretch 1st excited state of GdmSCN/KSCN=1/1 mixed crystal in melts at 403 K. Dots are data, and lines are single exponential fit.

cause $S^{13}C^{15}N^-$ anions are too far away to effectively exchange energy. Therefore, the molecular rotational time constant τ_{or} can be determined by fitting the anisotropy decay of the $S^{13}C^{15}N^-$ signal, which is 6.3±0.3 ps in this sample. In the 100% sample (GdmSCN/KSCN=1/1 mixed crystal in melt), the anisotropy decay of the SCN^- signal is from both molecular rotations and resonant energy transfers with a time constant τ, and it is determined to be 2.1±0.1 ps. Based on the above values, the resonant energy transfer time constant $\tau_e=1/(1/\tau-1/\tau_{or})$ is determined to be 3.2 ps. Thus, for sample GdmSCN/KS^{13}C^{15}N=1/1 salt in melt, the resonant energy transfer rate should be half of that in 100% sample, which means 6.4 ps (2×3.2), since the SCN^- (or $S^{13}C^{15}N^-$) anions are half of that in the sample GdmSCN/KSCN=1/1 mixed crystal in melt.

To measure the nonresonant energy transfers of nitrile stretches between SCN^- and $S^{13}CN^-$ with an energy donor/acceptor gap of 47 cm^{-1} and between SCN^- and $S^{13}C^{15}N^-$ with an energy donor/acceptor gap of 76 cm^{-1}, the vibrational energy exchange method [32, 33, 37, 40, 43] was used.

Figure 3 (a) and (b) display the waiting time dependent 2D IR spectra of sample GdmSCN/KS^{13}CN=1/1 and GdmSCN/KS^{13}C^{15}N=1/1 salt in melts at 403 K, respectively. Their FTIR spectra are shown in Fig.1 (c) and (d), respectively. At very short waiting time, *e.g.* 0 ps, there are two pairs of peaks on the diagonal positions. Peaks 1 and 2 are the CN stretch 0-1 and 1-2 transition peaks respectively, and peaks 3 and 4 are the corresponding transition peaks of the ^{13}CN (or $^{13}C^{15}N$) stretch, respectively. Small cross peaks arise from the vibrational coupling between the CN stretch and the ^{13}CN stretch, and between the CN stretch and the $^{13}C^{15}N$ stretch, respectively. With the waiting time increasing, the vibrational excitations of both nitrile stretches begin to exchange, which produces two pairs of peaks (peaks 5−8) on the off-diagonal positions (panel 30 ps). Peaks 5 and 6 originate from the energy transfer from the CN stretch 1st excited state

DOI:10.1063/1674-0068/29/cjcp1602028

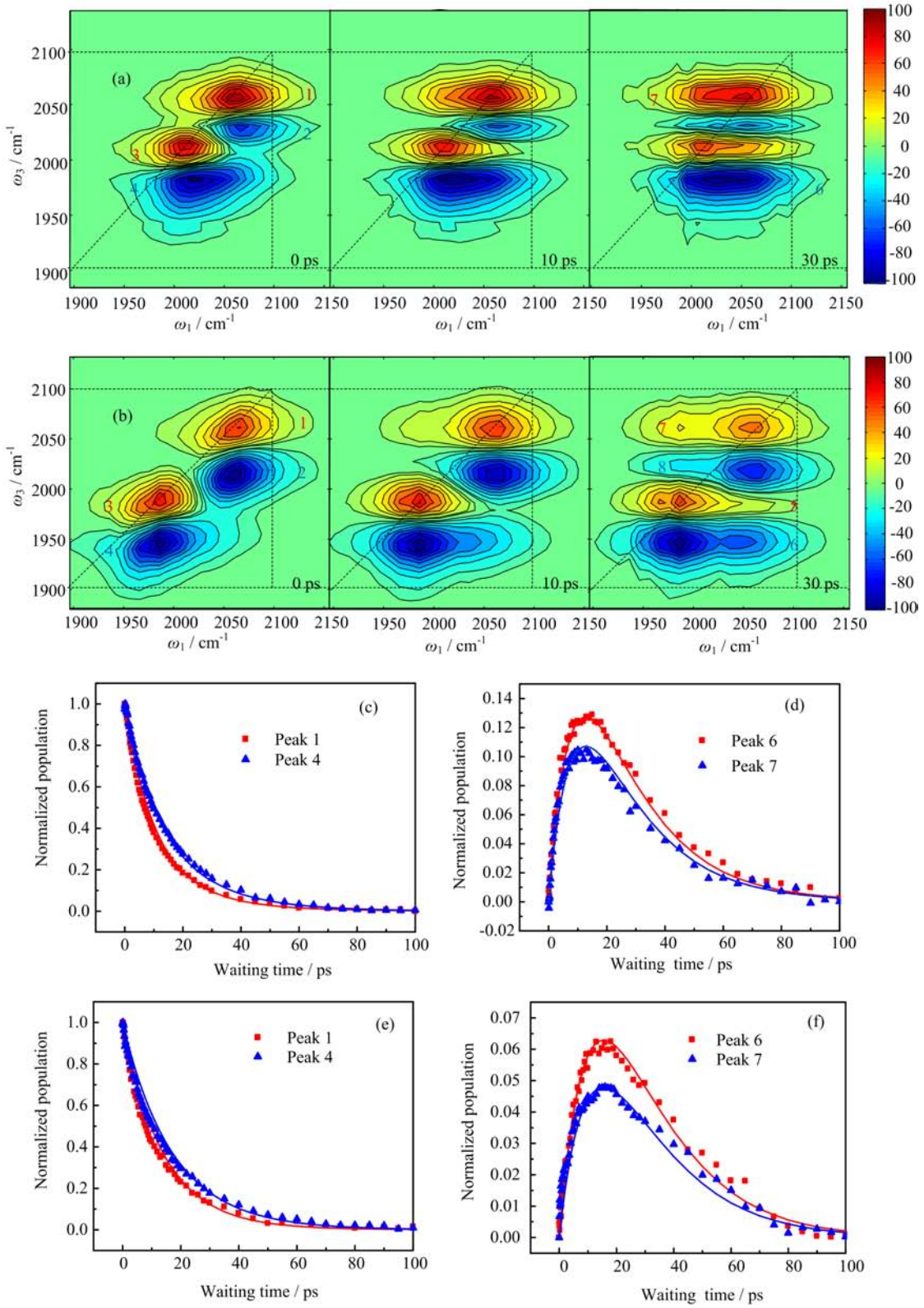

FIG. 3 (a) 2D IR spectra of GdmSCN/KS^{13}CN=1/1 mixed crystal in melts at 403 K at three waiting time of 0, 10, and 30 ps. (b) 2D IR spectra of GdmSCN/KS^{13}C^{15}N=1/1 mixed crystal in melts at 403 K at three waiting time of 0, 10, and 30 ps. The maximum intensity in each plot is normalized to be 1. (c) and (d) The waiting time dependent intensities of peaks 1, 4, 6, 7 in (a). (e) and (f) The waiting time dependent intensities of peaks 1, 4, 6, 7 in (b). Dots are experimental data, and curves are calculations based on the energy exchange model.

DOI:10.1063/1674-0068/29/cjcp1602028

to that of the ^{13}CN (or ^{13}C^{15}N) stretch, respectively. Peaks 7 and 8 originate from (i) the energy transfer from the ^{13}CN and ^{13}C^{15}N stretch, respectively, to the CN stretch 1st excited state, (ii) the vibrational coupling between the CN stretch and the ^{13}C stretch and between the CN stretch and the ^{13}C^{15}N stretch, respectively, and (iii) the heat-induced CN stretch absorption change. In this system, the heat effect is small due to the long vibration lifetime of CN stretch mode. The vibrational coupling between the CN and its isotopes has the dynamics similar to vibration decay of CN stretch. After properly removing the contributions from the vibrational coupling by generating the exponential curve in which the decay time is the same as the vibrational lifetime (the method was developed previously [31]), we can do quantitative analyses on the energy transfer kinetics. In Fig.3 (a) and (b), each diagonal peak pair and its corresponding cross peak pair along the y-axis form an energy donor (diagonal)/acceptor (cross) pair. The relative cross/diagonal peak ratio indicates how fast the vibrational energy transfers from the donor to the acceptor. By comparing Fig.3 (a) and (b), we can see that the cross peaks of SCN$^-$/S^{13}C^{15}N$^-$ (energy mismatch $\sim$76 cm^{-1}) are obviously smaller than those of the SCN$^-$/S^{13}CN$^-$ (energy mismatch $\sim$47 cm^{-1}) at the same waiting time. This simple inspection qualitatively reveals that a system with a bigger energy mismatch has a slower energy transfer rate.

From panels 10 and 30 ps (in Fig.3 (a) or (b)), it can be seen that the peak amplitude of 6 are larger than that of 7 at the same waiting time. This is because of the detailed balance principle, which requires that at equilibrium the populations at two energy levels fulfill the Boltzmann distribution. Therefore the energy down-flowing must be faster than the up-pumping process with a rate ratio determined by the Boltzmann factor.

For the GdmSCN/KS^{13}CN=1/1 sample in melt at 403 K, simultaneously analyzing the time dependent intensities of peaks 1, 4, 6, and 7 (after properly removing the contributions from the heat effect and the vibrational coupling) in Fig.3 (c) and (d) with the energy exchange kinetic model quantitatively gives the energy transfer time constant of down-flowing ($1/k_{\mathrm{CN}\rightarrow{}^{13}\mathrm{CN}}$) process to be 36$\pm$3 ps. The kinetic model description is provided in the supplementary material. Using the same procedure, for the GdmSCN/KS^{13}C^{15}N=1/1 sample in melts at 403 K, the energy transfer time constant of down-flowing ($1/k_{\mathrm{CN}\rightarrow{}^{13}\mathrm{C}^{15}\mathrm{N}}$) process is 90$\pm$9 ps. Data and fittings are displayed in Fig.3 (e) and (f).

In other words, with the energy gap increases from 0 to 47 cm^{-1} to 76 cm^{-1}, the energy transfer time increases from 6.4 ps to 36 ps to 90 ps.

If the energy transfers are through the dephasing mechanism, Eq.(1) must be able to describe both the resonant energy transfer and the two nonresonant energy transfer rates with the same parameters. Eq.(1) has only two unknown parameters (V and τ), and we have three sets of experimental data for k_{DA} and $\Delta\omega$. By fitting two sets of these experimental data, we can get the parameters ($V$and τ). The obtained parameters should predict the third set of experimental data. For example, by fitting the data 6.4 ps ($\Delta\omega$=0) and 36 ps ($\Delta\omega$=47 cm^{-1}) with Eq.(1), we obtain V=4.30 cm^{-1} and τ^{-1}=17.50 cm^{-1} with the calculated time constants 6.2 ps ($\Delta\omega$=0), 39.2 ps ($\Delta\omega$=47 cm^{-1}). Using the coupling strength and the dephasing width, the calculated energy transfer time constant for $\Delta\omega$=76 cm^{-1} is 88.90 ps. Within experimental uncertainty ($\sim$10%), the value is the same as experimental result. Here one issue needs to be emphasized. In converting the dephasing time τ with the line width (τ^{-1}) in the denominator of Eq.(1), a factor of 2π is needed, *e.g.* if τ^{-1}=17.50 cm^{-1}, τ must be $\tau=\dfrac{1}{2\pi}\dfrac{100}{17.5\times 3}$=0.30 ps.

Now, we need to evaluate whether the two obtained parameters V=4.30 cm^{-1} and τ^{-1}=17.50 cm^{-1} are in reasonable ranges. As discussed in previous work [37], the energy transfer dephasing line widths (τ^{-1}) must not be larger than the sum of the donor and acceptor absorption line widths. As determined in Fig.1 (e) and (f), the vibrational frequency of nitrile stretch in melts has a line width of 34 cm^{-1} at 403 K. The sum of line widths of the donor and acceptor is therefore 68 cm^{-1}. The determined energy transfer line width τ^{-1}=17.50 cm^{-1} is about 25.7% of the sum, indicating that the dephasings of the donor and acceptor are correlated.

In melts, because of no solvents separating the anions, all of anions are close to each other and hence can transfer energy efficiently. Therefore, the energy transfer rate measured is not simply the sum of transfers from one donor to many acceptors, but more like a chain reaction [37]. In other words, the energy may transfer from the donor to acceptor and from this acceptor to another anion, and so on, similar to those in the KSCN crystal [38]. As a result, it is difficult to precisely evaluate the coupling strength V=4.30 cm^{-1}. However, from the previous work [37, 39], we know that the structure of the clusters looks like that of the molten samples, and in the saturated KSCN/KS^{13}C^{15}N=1/1 D_2O solution the coupling strength is V=4.1 cm^{-1}. Because of the similarity between GdmSCN/KSCN=1/1 mixed crystal in melts and KSCN/KS^{13}C^{15}N=1/1 D_2O saturated solution, we can assume that the coupling strength V=4.30 cm^{-1} of GdmSCN/KSCN=1/1 in melt at 403 K is in reasonable range.

In summary, the experimental results suggest that the dephasing dominates the energy transfers in melts (phonon compensation mechanism was ruled out above). Eq.(1) of the dephasing mechanism quantitatively describes both resonant and nonresonant vibrational energy transfers in GdmSCN/KS^{13}CN=1/1 and GdmSCN/KS^{13}C^{15}N=1/1 mixed crystal in melts at 403 K very well.

DOI:10.1063/1674-0068/29/cjcp1602028

TABLE I Experimental and calculated resonant and nonresonant vibrational energy transfer time constants and calculated coupling strengths and dephasing widths in GdmSCN/KS^{13}CN=1/1 and GdmSCN/KS^{13}C^{15}N=1/1 melts at 403 and 473 K, respectively.

Sample		Vibrational energy transfer time constants/ps			Coupling/cm^{-1}	Linewidth/cm^{-1}
		$\Delta\omega$=0 cm^{-1}	$\Delta\omega$=47 cm^{-1}	$\Delta\omega$=76 cm^{-1}		
Melt (403 K)	Experimental data	6.4	36	90		
	Calculated values	6.2	39.2	88.9	4.3	17.5
Melt (473 K)	Experimental data	6.8	37	82		
	Calculated values	6.9	36.7	82.2	4.25	20

[a] Resonant vibrational energy transfer in GdmSCN/KS^{13}C^{15}N=1/1 mixed crystal in melts.
[b] Nonresonant vibrational energy transfer with an energy gap 47 cm^{-1} in GdmSCN/KS^{13}CN=1/1 mixed crystal in melts.
[c] Nonresonant vibrational energy transfer with an energy gap 76 cm^{-1} in GdmSCN/KS^{13}C^{15}N=1/1 mixed crystal in melts.

C. Temperature dependent vibrational energy transfers in melts

One of the interesting predictions of Eq.(1) is that the resonant energy transfer will become slower and the nonresonant energy transfer will become faster at a higher temperature if $\Delta\omega>\tau^{-1}>V$ (for $\Delta\omega\neq0$) and $\tau^{-1}>V$ (for $\Delta\omega=0$) and no chemical transformations occur within the temperature range, because at a higher temperature molecular motions are faster and the energy transfer dephasing caused by the motions typically becomes faster accordingly (τ^{-1} is larger at a higher temperature) [37]. Previous work on the resonant and nonresonant vibrational energy transfers in the KSCN/KS^{13}C^{15}N D_2O 10 mol/L solutions from room temperature to 80 °C are consistent with this prediction [37]. Then the question is raised as to whether these predictions will still work in melts. In this section, we focus on answering this question.

Figure 4(a) shows the anisotropy decay of the nitrile stretch ^{13}C^{15}N in sample GdmSCN/KSCN/KS^{13}C^{15}N=0.5/0.48/0.02 and CN in sampleGdmSCN/KSCN=1/1 as a function of waiting time in melts at 473 K, respectively. With the same procedure, by fitting the anisotropy decay of the S^{13}C^{15}N$^-$ in isotopic labeled sample GdmSCN/KSCN/KS^{13}C^{15}N=0.5/0.48/0.02, the molecular rotational time constant τ_{or} can be obtained to be 3±0.3 ps. In the 100% sample (GdmSCN/KSCN=1/1 mixed crystal in melts), the anisotropy decay time constant τ is determined to be 1.6±0.1 ps. Based on the above values, the resonant energy transfer time constant $\tau_e=1/(1/\tau-1/\tau_{or})$ is determined to be 3.4 ps. Thus, for sample GdmSCN/KS^{13}C^{15}N=1/1 salt in melts, the resonant energy transfer time should be 6.8 ps (2×3.4), since the SCN$^-$ (or S^{13}C^{15}N$^-$) anions are half of that in the sample GdmSCN/KSCN=1/1 mixed crystal in melts.

Using a similar procedure described above, we can also simultaneously analyze the time dependent intensities of diagonal peaks and cross peaks (shown in Fig.4 (b) and (c)). With the energy exchange kinetic model it gives the energy transfer time constant of downflowing ($1/k_{CN\rightarrow{}^{13}CN}$) process to be 37±3 ps. The details are provided in the supplementary materials. For the GdmSCN/KS^{13}C^{15}N=1/1 mixed crystal in melts at 473 K, the energy transfer time constant of downflowing ($1/k_{CN\rightarrow{}^{13}C^{15}N}$) process is 82±8 ps. Data and fittings are displayed in Fig.4 (d) and (e). Their FTIR spectra are shown in Fig.1 (e) and (f), respectively.

By fitting the two sets of experimental data 6.8 ps ($\Delta\omega$=0), 37 ps ($\Delta\omega$=47 cm^{-1}) with Eq.(1), we obtain the coupling strength V=4.25 cm^{-1} and the dephasing width τ^{-1}=20.00 cm^{-1} with the calculated time constants 6.90 ($\Delta\omega$=0), 36.70 ps ($\Delta\omega$=47 cm^{-1}). Using the coupling strength and the dephasing width, the calculated time constant for $\Delta\omega$=76 cm^{-1} is 82.20 ps. Again, within experimental uncertainty (∼10%), the calculated energy transfer time is identical with measured value. For comparison, data of the two melts are listed in Table I.

As shown in Table I, at 473 K, the resonant energy transfer time increases to 6.8 ps from 6.4 ps at 403 K, but that of the nonresonant energy transfer with an energy gap 76 cm^{-1} becomes faster to 82 ps from 90 ps. The opposite temperature dependence of resonant and nonresonant energy transfers are consistent with the prediction by Eq.(1). However, all the differences are within experimental uncertainty (∼10%). Especially, the nonresonant energy transfer time with an energy gap 47 cm^{-1} at 473 K is almost the same as that at 403 K. The possible reasons are that, in Eq.(1) the temperature T change causes the energy transfer rate k_{DA} to change little than that of $\Delta\omega$ and in our experiment the increase of temperature is still small. Based on the calculated values, we can know that the nonresonant energy transfer time with an energy gap 47 cm^{-1} becomes faster to 36.7 ps at 473 K from 39.2 ps at 403 K. The coupling strength at 473 K is almost the same as that at 403 K within experimental uncertainty. The almost same coupling strength indicates that the average anion distance at 473 K is similar to that at 403 K in the same sample, because the other parameters in Eq.(2) which correlate the coupling strength to

DOI:10.1063/1674-0068/29/cjcp1602028

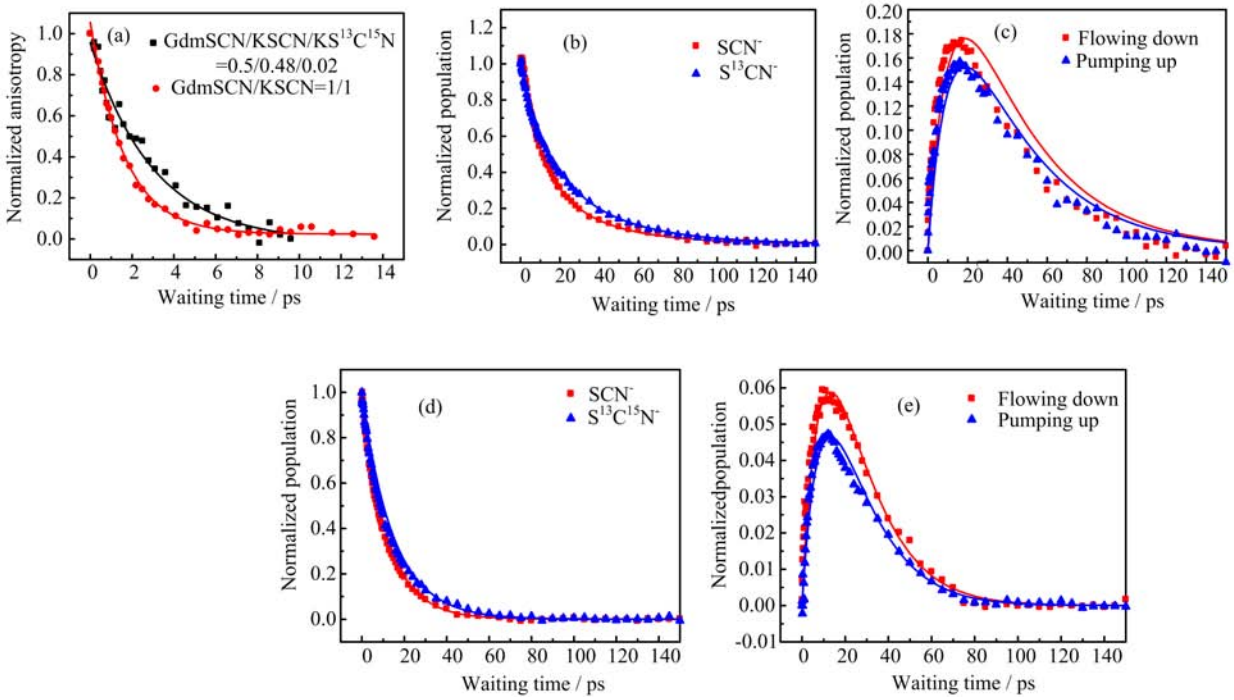

FIG. 4 (a) Anisotropy decay data of $^{13}C^{15}N$ stretch 1st excited state of 2% $KS^{13}C^{15}N$ in GdmSCN/KSCN/$KS^{13}C^{15}N$=0.5/0.48/0.02 mixed crystal in melts at 473 K, and of CN stretch 1st excited state of GdmSCN/KSCN=1/1 mixed crystal in melts at 473 K. Dots are data, and curves are fitted with single exponentials. (b) The waiting time dependent diagonal peak intensities of 0-1 transition peak (SCN^-) and of 1-2 transition peak ($S^{13}C^-$) (similar to peaks 1 and 4 in Fig.3(c)), (c) the waiting time dependent off-diagonal peak intensities of 1-2 transition peak ($S^{13}C^-$) and of 0-1 transition peak (SCN^-) (similar to peaks 6 and 7 in Fig.3(d)) of GdmSCN/$KS^{13}CN$=1/1 mixed crystal in melts at 473 K, (d) the waiting time dependent diagonal peakintensities of 0-1 transition peak (SCN^-) and of 1-2 transition peak ($S^{13}C^{15}N^-$) (similar to peaks 1 and 4 in Fig.3(e)), (e) the waiting time dependent off-diagonal peak intensities of 1-2 transition peak ($S^{13}C^{15}N^-$) and of 0-1 transition peak (SCN^-) (similar to peaks 6 and 7 in Fig.3(f) of GdmSCN/$KS^{13}C^{15}N$=1/1 mixed crystal in melts at 473 K. Dots are data and curves are kinetic model calculations.

the distance are weakly temperature dependent. This is consistent with the temperature dependent FTIR measurement (in Fig.1 (c)−(f)). The larger energy transfer dephasing line width indicates that the energy transfer dephasing at 473 K is faster. As discussed in the previous work [37], this is probably because the molecular motions are faster. This is supported by the faster molecular rotation (3 ps) at 473 K compared to that (6.3 ps) at 403 K.

In summary, using the two molten salts at two different temperatures, we have quantitatively tested the dephasing mechanism in melts, and demonstrate that the dephasing mechanism and its predictions are applicable.

D. Vibrational energy transfers in aqueous solutions

As discussed in the previous work [39, 40], in liquid (melt and solution), molecular motions (*e.g.* rotations and translations of a few angstroms) are much faster than the energy transfer process. Therefore, before the energy transfer occurs, the fast molecular motions can cause the positions or phases of the donor and acceptor relative to the phonons to fluctuate or even exchange. This significantly reduces the difference between the phonon modulations on the donor and the acceptor, causing the efficiency of phonon compensation for the D/A gap to diminish. As a result, in liquids the dephasing mechanism is dominant. We have demonstrated the GdmSCN/KSCN=1/1 system in melts can be described by the dephasing mechanism. In the following we will show the results of the systems in aqueous solutions.

As shown in Fig.5(a), the resonant energy transfer time in the GdmSCN/KSCN=1/1 D_2O saturated solution can be obtained from the rate difference between the 1/1 and 0.5/0.48/0.02 D_2O saturated solutions (1/(1/2.65−1/5.54)) to be 5.08 ps, which indicates that the resonant energy transfer time constant in the GdmSCN/$KS^{13}C^{15}N$ D_2O saturated solution would be 5.08×2≈11.2 ps as the number of acceptors is 50% fewer. Based on the 2DIR energy exchange measurements (Fig.5 (b)−(e)), the vibrational energy transfer time constant from CN to ^{13}CN in a GdmSCN/$KS^{13}CN$=1/1 D_2O saturated solution is determined to be 80±8 ps, and that from CN to $^{13}C^{15}N$ in a GdmSCN/$KS^{13}C^{15}N$=1/1 D_2O saturated solution

DOI:10.1063/1674-0068/29/cjcp1602028

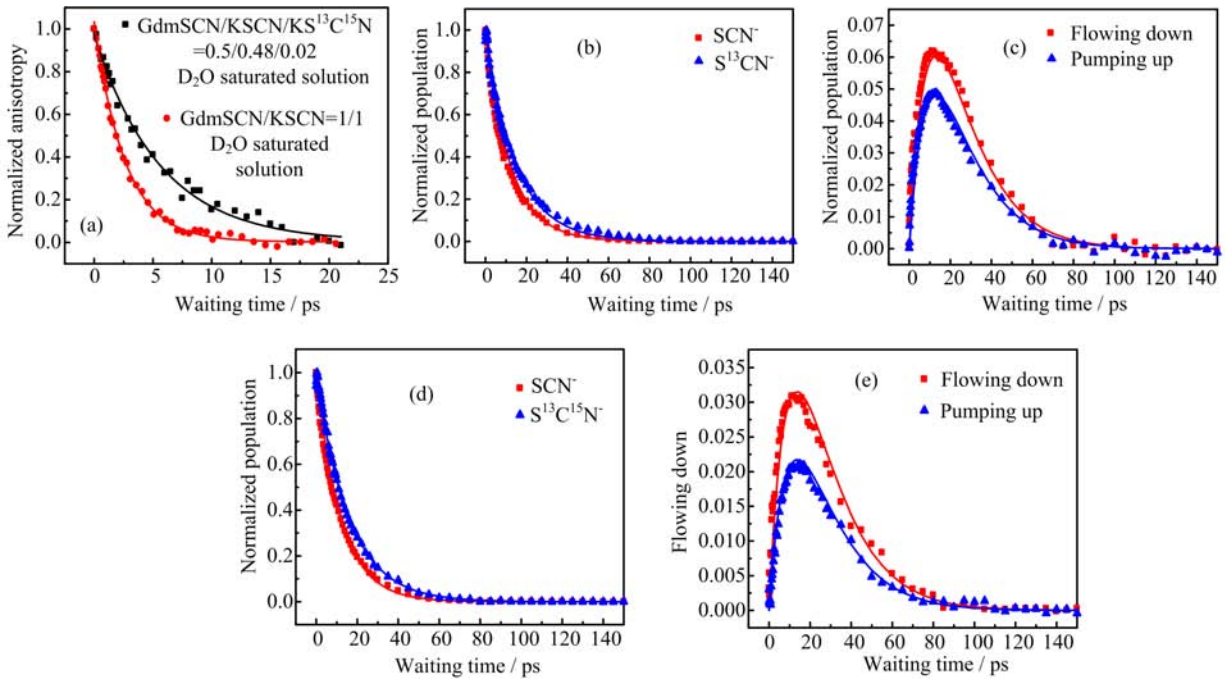

FIG. 5 (a) Anisotropy decay data of $^{13}C^{15}N$ stretch 1st excited state of 2% $KS^{13}C^{15}N$ in GdmSCN/KSCN/$KS^{13}C^{15}N$=0.5/0.48/0.02 D_2O saturated solution at 296 K, and that of CN stretch 1st excited state of GdmSCN/KSCN=1/1 D_2O saturated solution at 296 K. Dots are data, and curves are fitted with single exponentials. (b) The waiting time dependent diagonal peak intensities of 0-1 transition peak (SCN^-) and of 1-2 transition peak ($S^{13}C^-$) (similar to peaks 1 and 4 in Fig.3(c)), (c) the waiting time dependent off-diagonal peak intensities of 1-2 transition peak ($S^{13}C^-$) and of 0-1 transition peak (SCN^-) (similar to peaks 6 and 7 in Fig.3(d)) of GdmSCN/$KS^{13}CN$=1/1 D_2O saturated solution at 296 K, (d) the waiting time dependent diagonal peak intensities of 0-1 transition peak (SCN^-) and of 1-2 transition peak ($S^{13}C^{15}N^-$) (similar to peaks 1 and 4 in Fig.3(e)), (e) the waiting time dependent off-diagonal peak intensities of 1-2 transition peak ($S^{13}C^{15}N^-$) and of 0-1 transition peak (SCN^-) (similar to peaks 6 and 7 in Fig.3(f)) of GdmSCN/$KS^{13}C^{15}N$=1/1 D_2O saturated solution at 296 K. Dots are data and curves are kinetic model calculations.

is determined to be 160±10 ps. The kinetic model description is provided in the supplementary material. By fitting the two sets of experimental data 11.2 ps ($\Delta\omega$=0), 80 ps ($\Delta\omega$=47 cm^{-1}) with Eq.(1), we obtain the coupling strength V=3.05 cm^{-1} and the dephasing width τ^{-1}=18.20 cm^{-1} with the calculated time constants 11.5 ps ($\Delta\omega$=0), 72.60 ps ($\Delta\omega$=47 cm^{-1}). Using the coupling strength and the dephasing width, the calculated time constant for $\Delta\omega$=76 cm^{-1} is 163.00 ps. Again, within experimental uncertainty (∼10%), the calculated energy transfer time is identical to measured value. The results show that the nonresonant energy transfer rates in solutions are strongly dependent on the energy gap. The vibrational energy transfer between the nitrile stretches is faster with a smaller energy donor/acceptor gap. We can also notice that the coupling strength in the solutions (3.5 cm^{-1}) is slightly smaller than that in melts (4.3 cm^{-1}), indicating that the average anion distance in the solutions are slightly larger than that in melts probably because of the water solvation.

In summary, using the same systems in solution at 296 K, we confirm the dephasing mechanism is also applicable for the mixed crystals in solutions.

E. Vibrational energy transfer in melts and solutions cannot be described by phonon compensation mechanism

As discussed in our previous work [40], for the one-phonon process, the first order coupling matrix [46] is used by the majority of theoretical approaches:

$$k_{\mathrm{DA}} = V_{\mathrm{DA}}^2 {V'_{\mathrm{s\text{-}b}}}^2 \rho_{\Delta E_{\mathrm{DA}}} N \tag{5}$$

where k_{DA} is the energy transfer rate constant from donor (D) to acceptor (A). ΔE_{DA} is the donor/acceptor energy gap. V_{DA} is the coupling between donor and acceptor. $V'_{\mathrm{s\text{-}b}}$ is the system-bath coupling. $\rho_{\Delta E_{\mathrm{DA}}}$ is the phonon density of the bath at the energy gap ΔE_{DA}. For the emission process,

$$N = \left[\exp\left(\frac{|\Delta E_{\mathrm{DA}}|}{RT} - 1\right)\right]^{-1} + 1 \tag{6}$$

and for the absorption process,

$$N = \left[\exp\left(\frac{|\Delta E_{\mathrm{DA}}|}{RT} - 1\right)\right]^{-1} \tag{7}$$

Meanwhile, there is also another theoretical approach [46] stating that the first order coupling matrix is very

DOI:10.1063/1674-0068/29/cjcp1602028

TABLE II Experimental and predicted energy transfer rate ratios $k_{CN\rightarrow{}^{13}CN}$ (47 cm^{-1}) /$k_{CN\rightarrow{}^{13}CN}$ (76 cm^{-1}).

	Experiments	Prediction		
		Eq.(1)	Eq.(5)	Eq.(8)
Melt (403 K)	2.50/1	2.27/1	$1.54x_1$/1	$4.02x_1$/1
Melt (473 K)	2.22/1	2.24/1	$1.55x_2$/1	$4.05x_2$/1
In D_2O (296 K)	2.00/1	2.25/1	$1.51x_3$/1	$3.95x_3$/1

Note: x_1=$\rho_{47\ cm^{-1}}/\rho_{76\ cm^{-1}}$ in melt at 403 K, x_2=$\rho_{47\ cm^{-1}}/\rho_{76\ cm^{-1}}$ in melt at 473 K. x_3=$\rho_{47\ cm^{-1}}/\rho_{76\ cm^{-1}}$ in D_2O saturated solution at 296 K.

close to zero. Therefore, the second order coupling matrix rather than the first one is needed to describe the one-phonon process [37, 40]:

$$k_{DA} = V_{DA}^2 V_{s\text{-}b}'^2 \frac{\rho_{\Delta E_{DA}}}{\Delta E_{DA}^2} N \quad (8)$$

The above two energy transfer equations (Eq.(5) and Eq.(8)) to describe the same process are similar except that there is a term ΔE_{DA}^2 in the denominator of Eq.(8) which makes the prediction on the gap dependence of energy transfer rate different from that by Eq.(5).

In our previous work [40], we have demonstrated that V_{DA} and $V'_{s\text{-}b}$ are independent of the energy gap for the systems they studied. The ratio of $\rho_{\Delta E_{DA}}$ ($\rho_{47\ cm^{-1}}/\rho_{76\ cm^{-1}}$) at different gaps for the systems we studied is assumed to be x_1 (in melt at 403 K), x_2 (in melt at 473 K), and x_3 (in D_2O saturated solution at 296 K). The parameter, N, is gap dependent. For the emission processes with gaps 47 and 76 cm^{-1}, the ratios of $N(47\ cm^{-1})/N(76\ cm^{-1})$ are 1.54/1 (melt at 403 K), 1.55/1 (melt at 473 K), and 1.51/1 (D_2O solution at 296 K), respectively. Summarizing the above discussions, the energy gap dependence of the vibrational energy transfer rate constants predicted by Eq.(5) and Eq.(8) are listed in Table II. For comparison, we also list the experimental energy transfer rate ratios and that reproduced by Eq.(1) in Table II.

To estimate the photon densities, we measured the Raman spectra of samples. Figure 6(a) displays the Raman spectrum of GdmSCN/KSCN=1/1 H_2O saturated solution at 296 K. Figure 6(b) displays the Raman spectrum of GdmSCN/KSCN=1/1 in melts at 403 K. The peak intensity increases from 50 cm^{-1} to 80 cm^{-1} in a continuous way. In addition, the isotope labeling does not change the internal vibrational modes of SCN^- at frequencies below 100 cm^{-1} where the energy gaps among the nitrile stretches are (their corresponding Raman spectra are provided in supplementary material), because no internal vibrational modes of the SCN^- reside at such low frequencies.

If the relative phonon densities are proportional to the Raman spectral intensities at different frequencies (which is a reasonable assumption for many cases), x_1 and x_2 can be determined to be <50% (melts) and x_3<30% (D_2O solution), according to the Raman spectra in Fig.6. As shown in Table II, the predictions

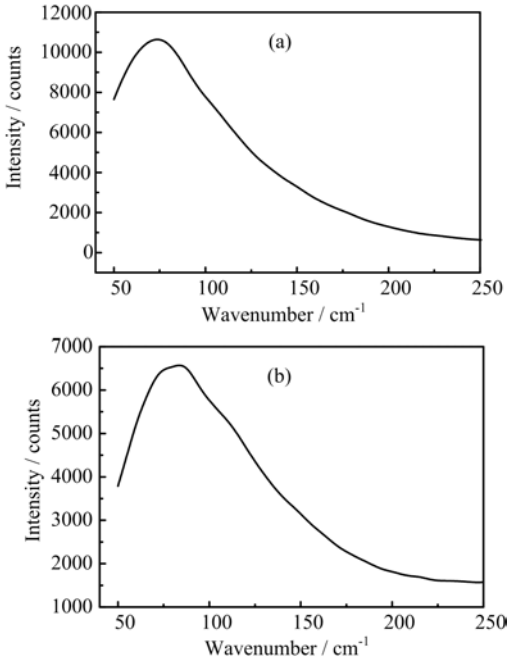

FIG. 6 (a) Raman scattering spectrum of GdmSCN/KSCN=1/1 H_2O solution at 296 K. (b) Raman scattering spectrum of GdmSCN/KSCN=1/1 in melts at 403 K.

of Eq.(5) are off from the experimental results largely. Meanwhile, the predictions of Eq.(8) cannot reproduce the experimental results perfectly as Eq.(1).

Summarizing the above discussion, we can see that the prediction of either Eq.(5) or Eq.(8) cannot describe all the experimental results. However, it can be quantitatively described by the dephasing mechanism.

IV. CONCLUSION

In this work, we systematically studied intermolecular vibrational energy transfers in the same systems in melts at two different temperatures and in solutions at room temperature, respectively. Experimental results suggest that in both melts and solutions both resonant and nonresonant intermolecular vibrational energy transfers are dominated by the dephasing mechanism. In both types of samples, the energy transfer is faster

DOI:10.1063/1674-0068/29/cjcp1602028

with a smaller donor/acceptor energy gap, independent of the Raman spectra. The energy gap dependences of the nonresonant energy transfers cannot be described by the phonon compensation mechanisms with the assumption that the relative phonon densities are similar to the Raman spectra. Instead, the experimental energy gap dependences can be quantitatively reproduced by the dephasing mechanism. The results also suggest that local structures, phonon modes and densities, and molecular motions in the molten salts at the time scales of a few to hundreds of ps are different from those in corresponding crystals.

Supplementary materials: The kinetic model of energy transfer and experimental data analysis process are given.

V. ACKNOWLEDGMENTS

This work was supported by the National Natural Science Foundation of China (No.21373213), the Chinese Academy of Sciences, and the Ministry of Science and Technology. Jun-rong Zheng is supported by the AFOSR Award No.FA9550-11-1-0070, the Welch foundation under Award No.C-1752, the David and Lucile Packard Foundation for a Packard fellowship, and the Alfred P. Sloan Foundation for a Sloan fellowship.

[1] C. B. Harris, D. E. Smith, and D. J. Russell, Chem. Rev. **90**, 481 (1990).
[2] D. D. Dlott, Chem. Phys. **266**, 149 (2001).
[3] E. J. Heilweil, M. P. Casassa, R. R. Cavanagh, and J. C. Stephenson, J. Chem. Phys. **85**, 5004 (1986).
[4] E. J. Heilweil, R. R. Cavanagh, and J. C. Stephenson, J. Chem. Phys. **89**, 230 (1988).
[5] M. Tuckerman and B. J. Berne, J. Chem. Phys. **98**, 7301 (1993).
[6] V. M. Kenkre, A. Tokmakoff, and M. D. Fayer, J. Chem. Phys. **101**, 10618 (1994).
[7] D. W. Miller and S. A. Adelman, Int. Rev. Phys. Chem. **13**, 359 (1994).
[8] A. Tokmakoff, B. Sauter, and M. D. Fayer, J. Chem. Phys. **100**, 9035 (1994).
[9] R. Rey and J. T. Hynes, J. Chem. Phys. **104**, 2356 (1996).
[10] H. Graener, R. Zurl, and M. Hofmann, J. Phys. Chem. B **101**, 1745 (1997).
[11] J. C. Deak, L. K. Iwaki, S. T. Rhea, and D. D. Dlott, J. Raman Spectrosc. **31**, 263 (2000).
[12] G. Seifert, R. Zurl, T. Patzlaff, and H. Graener, J. Chem. Phys. **112**, 6349 (2000).
[13] E. L. Sibert and R. Rey, J. Chem. Phys. **116**, 237 (2002).
[14] Z. H. Wang, A. Pakoulev, and D. D. Dlott, Science **296**, 2201 (2002).
[15] J. C. Deak, Y. S. Pang, T. D. Sechler, Z. H. Wang, and D. D. Dlott, Science **306**, 473 (2004).
[16] P. B. Graham, K. J. M. Matus, and R. M. Stratt, J. Chem. Phys. **121**, 5348 (2004).
[17] A. Ma and R. M. Stratt, J. Chem. Phys. **121**, 11217 (2004).
[18] G. Hanna and E. Geva, J. Phys. Chem. B **112**, 15793 (2008).
[19] D. M. Leitner, Annu. Rev. Phys. Chem. **59**, 233 (2008).
[20] H. Fujisaki, K. Yagi, J. E. Straub, and G. Stock, Int. J. Quantum Chem. **109**, 2047 (2009).
[21] I. V. Rubtsov and R. M. Hochstrasser, J. Phys. Chem. B **106**, 9165 (2002).
[22] D. V. Kurochkin, S. R. G. Naraharisetty, and I. V. Rubtsov, Proc. Natl. Acad. Sci. USA **104**, 14209 (2007).
[23] M. Schade, A. Moretto, M. Crisma, C. Toniolo, and P. Hamm, J. Phys. Chem. B **113**, 13393 (2009).
[24] N. I. Rubtsova and I. V. Rubtsov, Annu. Rev. Phys. Chem. **66**, 717 (2015).
[25] H. M. Muller-Werkmeister and J. Bredenbeck, Phys. Chem. Chem. Phys. **16**, 3261 (2014).
[26] A. L. Le Sueur, R. E. Horness, and M. C. Thielges, Analyst **140**, 4336 (2015).
[27] M. S. Lynch, K. M. Slenkamp, and M. Khalil, J. Chem. Phys. **136**, 241101 (2012).
[28] M. Yang, F. Li, and J. L. Skinner, J. Chem. Phys. **135**, 10 (2011).
[29] J. L. Skinner, Theor. Chem. Acc. **128**, 147 (2011).
[30] H. Bian, J. Li, X. Wen, and J. Zheng, J. Chem. Phys. **132**, 184505 (2010).
[31] H. Bian, X. Wen, J. Li and J. Zheng, J. Chem. Phys. **133**, 034505 (2010).
[32] H. Bian, H. Chen, J. Li, X. Wen, and J. Zheng, J. Phys. Chem. A **115**, 11657 (2011).
[33] H. T. Bian, X. W. Wen, J. B. Li, H. L. Chen, S. Z. Han, X. Q. Sun, J. A. Song, W. Zhuang, and J. R. Zheng, Proc. Natl. Acad. Sci. USA **108**, 4737 (2011).
[34] H. Bian, J. Li, Q. Zhang, H. Chen, W. Zhuang, Y. Q. Gao, and J. Zheng, J. Phys. Chem. B **116**, 14426 (2012).
[35] J. Li, H. Bian, X. Wen, H. Chen, K. Yuan, and J. Zheng, J. Phys. Chem. B **116**, 12284 (2012).
[36] J. Li, H. Bian, H. Chen, X. Wen, B. T. Hoang, and J. Zheng, J. Phys. Chem. B **117**, 4274 (2013).
[37] H. Chen, X. Wen, X. Guo, and J. Zheng, Phys. Chem. Chem. Phys. **16**, 13995 (2014).
[38] H. Chen, X. Wen, J. Li, and J. Zheng, J. Phys. Chem. A **118**, 2463 (2014).
[39] H. Chen, H. Bian, J. Li, X. Wen, Q. Zhang, W. Zhuang, and J. Zheng, J. Phys. Chem. B **119**, 4333 (2015).
[40] H. Chen, Q. Zhang, X. Guo, X. Wen, J. Li, W. Zhuang, and J. Zheng, J. Phys. Chem. A **119**, 669 (2015).
[41] S. Woutersen and H. J. Bakker, Nature **402**, 507 (1999).
[42] G. D. Scholes, Annu. Rev. Phys. Chem. **54**, 57 (2003).
[43] H. L. Chen, H. T. Bian, J. B. Li, X. W. Wen, and J. R. Zheng, Int. Rev. Phys. Chem. **31**, 469 (2012).
[44] K. Yuan, H. Bian, Y. Shen, B. Jiang, J. Li, Y. Zhang, H. Chen, and J. Zheng, J. Phys. Chem. B **118**, 3689 (2014).
[45] Y. Shen, T. Wu, B. Jiang, G. Deng, J. Li, H. Chen, X. Guo, C. Ge, Y. Chen, J. Hong, X. Yang, K. Yuan, W. Zhuang, and J. Zheng, J. Phys. Chem. B **119**, 9893 (2015).
[46] S. A. Egorov and J. L. Skinner, J. Chem. Phys. **103**, 1533 (1995).

DOI:10.1063/1674-0068/29/cjcp1602028